AIAA JOURNAL
Vol. 36, No. 2, February 1998

Computational Analysis of Hypersonic Turbulent Flows over a Projectile with Aerospike

Venkata S. Krishnamurty* and Wei Shyy†
University of Florida, Gainesville, Florida 32611

The effects of compressibility and nonequilibrium in hypersonic turbulent flows are analyzed in the k–ε-based modeling framework with emphasis on the influence of factors such as streamline curvature and shock discontinuities. The flow past a projectile, with and without a drag reduction spike, is investigated to assess the various modeling issues and to shed light on the merit of this interesting aerodynamic concept. The importance of an account for the compressibility and nonequilibrium effects is demonstrated. Regarding the merit of the spike/aerodisk assembly, it is observed that although the addition of the spike reduces the pressure at the nose of the projectile by a factor of 10 it only results in a marginal reduction in the temperature.

I. Introduction

THE effects of compressibility on the evolution of a turbulent shear layer has been extensively studied and a review of these effects is presented in Ref. 1. Direct numerical simulation (DNS) studies of Zeman[2] and Sarkar et al.[3] seem to indicate that the effect of compressibility on both decaying compressible turbulence and homogeneous shear turbulence is a dissipative one. The modifications for the extra dissipation due to dilatational effects and the pressure dilatation correlation have been successful in predicting the reduction in growth rate and reduction in magnitudes of turbulence correlation coefficients of free shear layers.[4] But these modifications have been shown to aggravate the deficiencies of the eddy viscosity models in predicting the growth of turbulent wall shear layers.[5,6]

Krishnamurty and Shyy[7] have examined the equations that describe the evolution of a compressible turbulent flowfield and identified additional terms that had not been suitably accounted for. These are the turbulent mass flux term (and, hence, the enthalpic production) and the effect of the baroclinic term. Modifications have been proposed to account for these terms with the aim of solving the governing equations in their exact form.

In addition, modifications have been proposed[8,9] to suitably modify the constants in the transport equation for the rate of dissipation of turbulent kinetic energy (TKE). These modifications have been proposed to address turbulent flowfields where the rate of production of TKE and the rate of dissipation of TKE are not in equilibrium (this is an implicit assumption in the eddy viscosity-based models).

In Ref. 7, the set of modifications given in Table 1 (Refs. 8–12) have been evaluated through predictions made of the supersonic flow past an axisymmetric afterbody. The computational study of the flow past an axisymmetric afterbody indicated that the impact of the modifications for the turbulent mass flux (and thereby the enthalpic production) and the baroclinic torque was not significant in terms of the predictions made of the mean flowfield. Possible reasons for this observation could be that these terms are of an order of magnitude smaller than the other terms (in the respective transport equation) or that the compressibility effects are not really a major factor in the development of these shear layers. The latter reason could have played a more important role in the results obtained for the axisymmetric afterbody flowfield. The flowfield (the baseflow) is at an inlet Mach number of 2.46, modest for compressibility effects to play a major role in the development of the shear layer. In addition, as was pointed out in the earlier section, two different flow structures seem to determine the evolution of the shear layer downstream of the afterbody. These are the recirculating region and the free shear layer. The interaction of the developing free shear layer with the recirculating, low-speed fluid makes a major contribution to the production of energy for the turbulent fluctuations. The motivation for the current study stemmed from the need to clarify the issues raised by the observations from the predictions made of the axisymmetric afterbody flowfield. The other major interest of the present effort is the evaluation of the usefulness of the aerospike concept to reduce strong pressure and high temperature experienced on the surface of a hypersonic projectile.

The organization is as follows. In Sec. II, a description is given of the projectile flowfield that is being considered for computational analysis. Section III presents the equations of motion and presents a terse description of the modeling framework that has been adopted to test the various modifications. Section IV presents the computational study along with a discussion of the results obtained for both the spike-off case as well as the spike-on case. Section V concludes with a summary of the observations that have been made.

II. Projectile Forebody Flowfield

The flowfield is shown in Fig. 1. The strong shock ahead of the dome of the projectile causes a large increase in the pressure and temperature on the surface of the hemispherical dome. In addition to the increased drag on the projectile, these cause adverse conditions for the optical and other sensing equipment typically mounted in the dome of the projectile (due to the excessive heating of the dome surface). The experiments conducted by Huebner et al.[13] were intended to investigate the effect of a long slender spike and an aerodisk combination. This flow structure is shown in Fig. 2. The recirculating regions upstream of the dome drastically reduce the pressures and to a certain extent the temperature on the dome surface.

The relevant flow structure of the turbulent flowfield we are considering in this case is the interaction of the isotropic turbulence with the bow shock ahead of the dome of the projectile. Additionally, effects of the turbulent wall layer that separates upstream of the shoulder (the shoulder formed at the junction of the dome and the cylinder) and the expansion fan (Fig. 1) need to be considered in the analysis of the flowfield. A review of our current understanding of shock–turbulence interaction is presented in Ref. 1

Several experimental studies have been conducted to investigate the projectile forebody flowfield. Most of these studies, in the 1950s, concentrated on the issues of strong pressures and heating rates at the dome of the projectile and the means to reduce them. Stalder and Nielsen[14] conducted experiments on a simple hemisphere-cylinder configuration similar to the one shown in Fig. 3 at Mach numbers of 1.75, 2.67, and 5.0. Their experiments indicated a reduction in the pressure (consequently, the drag) on the surface of the dome,

Received March 20, 1997; revision received Sept. 3, 1997; accepted for publication Sept. 15, 1997.

*Graduate Student, Department of Aerospace Engineering, Mechanics, and Engineering Science; currently Staff Engineer, Kohler Co., Mail Stop 077, 444 Highland Drive, Kohler, WI 58044. Member AIAA.

†Professor and Chair, Department of Aerospace Engineering, Mechanics, and Engineering Science. Associate Fellow AIAA.

Table 1 Modifications to be evaluated

Modifications	Details	Author(s)
Nonequilibrium	Modification for 1) imbalance between production of TKE and its dissipation rate and 2) added timescale	Chen and Kim,[8] Shyy et al.,[12] and Thakur et al.[9]
Sarkar et al.[3]	Modification for 1) dilatational dissipation and 2) pressure dilatation terms	Sarkar et al.[3] and Sarkar[10]
El Baz and Launder[11]	Modification for 1) compressibility effects and 2) pressure dilatation term	El Baz and Launder[11]
Krishnamurty and Shyy[7]	Modifications for 1) turbulent mass flux and 2) baroclinic torque	Krishnamurty and Shyy[7] and Shyy et al.[12]

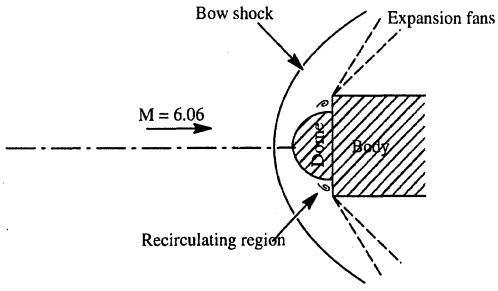

Fig. 1 Projectile forebody problem.

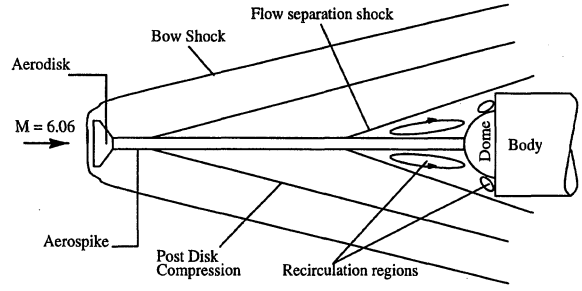

Fig. 2 Schematic of aerospike induced flowfield.

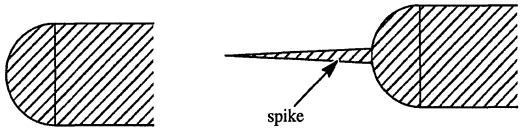

Hemisphere cylinder **Hemisphere cylinder with spike**

Fig. 3 Projectile configurations investigated by Stalder and Nielsen.[14]

with the addition of the spike. It did not, however, show a reduction in the temperature on the nose of the projectile. In fact, it showed an increase in heat transfer rates with the addition of the spike (in comparison with the unspiked case). They explained the increase in heat transfer rates as a result of the separated turbulent boundary layer (upstream of the nose) periodically impinging on the outer region of the boundary layer on the nose of the hemisphere.[14]

The experimental investigations of Bogdonoff and Vas[15] indicated an initial drop in the pressure at the nose of the forebody with increase in spike length (upto about $L/D = 3$) but asymptotes with any further increase in the spike length. The experimental investigation of Crawford[16] was chiefly concerned with the phenomenon of flow transition (from laminar to turbulent).

More recently, Huebner et al.[13] investigated the projectile flowfield. They conducted experimental measurements of the pressure and temperature at the nose of the projectile and the effect of the aerospike and aerodisk assembly (the flowfields investigated are given in Figs. 1 and 2) at various angles of attack.[13] They observe that at moderate angles of attack ($\alpha \leq 15$ deg) the spike and aerodisk assembly is very useful in reducing the pressure and temperature distributions on the surface of the dome. But at higher angles of attack the combination aggravates the situation at the dome surface with the shock impinging directly on the boundary layer on the dome surface.

III. Modeling Technique

In the solution of turbulent flowfields the variables are usually split into a mean and a fluctuating part. The mean can be defined in one of two ways: 1) Reynolds average or 2) Favre average. In solving for compressible flows, the use of Reynolds average introduces correlations involving density fluctuations and the modeling of these correlations is difficult. To overcome this a combination of Reynolds and mass-weighted Favre average is used. The advantage in doing this is that the governing equations bear a closer resemblance to their incompressible counterparts.

The equations representing conservation of mass, momentum, and energy in their averaged form are given next, where density and pressure are Reynolds averaged, whereas Favre averaging is used to define the mean of the velocity components and temperature. A tilde denotes a Favre-averaged quantity and a double prime denotes fluctuations with respect to the Favre mean. An overbar denotes a Reynolds average, and a prime denotes fluctuations with respect to it. The variables are split up into their mean and fluctuating part as

$$\varrho = \bar{\varrho} + \varrho', \quad u_i = \tilde{U}_i + u_i'', \quad T = \tilde{T} + T'', \quad p = P + p' \tag{1}$$

where ϱ, u_i, T, and p are the instantaneous density, velocity, temperature, and pressure, respectively. P is the Reynolds-averaged pressure. The equations in their averaged form are written as follows.

Continuity:

$$\frac{\partial}{\partial t}(\bar{\varrho}) + \frac{\partial}{\partial x_j}(\bar{\varrho}\tilde{U}_j) = 0 \tag{2}$$

Momentum:

$$\frac{\partial}{\partial t}(\bar{\varrho}\tilde{U}_j) + \frac{\partial}{\partial X_j}(\bar{\varrho}\tilde{U}_i\tilde{U}_j) = -\frac{\partial P}{\partial X_i} + \frac{\partial}{\partial X_j}[\Sigma_{ij} - \underbrace{\overline{\varrho u_i'' u_j''}}_{\text{A}}] \tag{3}$$

Energy:

$$\frac{\partial}{\partial t}(\bar{\varrho}\tilde{E}) + \frac{\partial}{\partial X_j}(\bar{\varrho}\tilde{U}_j\tilde{H}) = \frac{\partial}{\partial X_j}\left[\begin{array}{l} \tilde{U}_j(\Sigma_{ij} + \underbrace{\overline{\sigma_{ij}''}}_{\text{B}} - \underbrace{\overline{\varrho u_i'' u_j''}}_{\text{C}}) + \underbrace{\overline{u_i'' \sigma_{ij}''}}_{\text{D}} - \tilde{q}_j \\ \qquad - \underbrace{\overline{\varrho u_j'' h''}}_{\text{E}} - \underbrace{\overline{\varrho u_j''(\tfrac{1}{2} u_i'' u_i'')}}_{\text{F}} \end{array}\right] \tag{4}$$

TKE:

$$\frac{\partial}{\partial t}(\bar{\varrho}k) + \frac{\partial}{\partial x_j}(\bar{\varrho}\tilde{U}_i k) = \underbrace{-\overline{\varrho u_i'' u_j''}\frac{\partial \tilde{U}_i}{\partial x_j}}_{\text{G}} \underbrace{- \overline{u_i''}\frac{\partial P}{\partial x_i}}_{\text{H}} \underbrace{- \overline{\frac{\partial u_i''}{\partial x_j}\sigma_{ij}''}}_{\text{I}}$$

$$+ \frac{\partial}{\partial x_j}\left[\underbrace{\overline{u_i''\sigma_{ij}'' - \varrho u_j''(\tfrac{1}{2}u_i'' u_i'')}}_{\text{J}} - \overline{p' u_j''}\right] + \underbrace{\overline{p'\frac{\partial u_i''}{\partial x_i}}}_{\text{K}} \tag{5}$$

where

$$\Sigma_{ij} = 2\mu S_{ij} + \lambda \tilde{U}_{k,k}\delta_{ij}, \qquad S_{ij} = \tfrac{1}{2}(\tilde{U}_{i,j} + \tilde{U}_{j,i}) \tag{6}$$

$$\overline{\sigma_{ij}''} = 2\mu s_{ij} + \lambda \overline{u_{k,k}''}\delta_{ij}, \qquad s_{ij} = \tfrac{1}{2}(\overline{u_{i,j}''} + \overline{u_{j,i}''}) \tag{7}$$

E and H are the mass-weighted averages of specific total energy and specific total enthalpy, respectively, and are written as

$$E = e + \tfrac{1}{2}U_i U_i + \tfrac{1}{2}\overline{u_i'' u_i''} \tag{8}$$

$$\varrho H = \varrho E + p \tag{9}$$

and k represents the TKE and is equal to $k = \frac{1}{2}(\overline{\varrho u_i'' u_i''}/\bar{\varrho})$.

In the preceding equations, the terms that need to be modeled are indicated by a bracket and are labeled A–K. The current modeling procedure (of these terms) based on the k–ε model is given as follows.

Terms A, C, and G are the Reynolds stress terms. They are modeled as

$$-\overline{\varrho u_i'' u_j''} \simeq 2\mu_t S_{ij} + \lambda_t \frac{\partial U_k}{\partial x_k}\delta_{ij} - \frac{2}{3}\varrho k \delta_{ij} \tag{10}$$

where S_{ij} is defined in Eq. (6), μ_t is the eddy viscosity, and $\lambda_t = -\frac{2}{3}\mu_t$. Throughout we use capitalized notation to indicate averaged quantities (except for density, where ϱ will denote the average value). Implicit in the notation used is that the pressure and density are Reynolds averaged, whereas the velocity components and temperature are Favre averaged.

Terms D, F, and J represent the diffusion of energy due to turbulent fluctuations and are modeled as

$$\overline{u_i'' \sigma_{ij}''} - \overline{\varrho u_i''\left(\frac{1}{2}u_i'' u_i''\right)} \simeq \frac{\mu_t}{\sigma_k}\frac{\partial k}{\partial x_j} \tag{11}$$

The effect of the term $\overline{p' u_j''}$ on the rate of change of TKE is not explicitly accounted for and is included in the model for the diffusion terms given in Eq. (11).

Term E represents the turbulent heat flux, and using the Reynolds' analogy[17] this term is modeled as

$$-\overline{\varrho u_j'' h''} = \frac{\mu_t}{Pr_t}\frac{\partial T}{\partial x_j} \tag{12}$$

where Pr_t is the turbulent Prandtl number and is usually specified to be equal to 0.9.

Term I represents the rate of dissipation of turbulent kinetic energy due to molecular effects and is solved for via a transport equation. That is,

$$\overline{\frac{\partial u_i''}{\partial x_j}\sigma_{ij}''} = \varrho\varepsilon \tag{13}$$

In the k–ε-based modeling, transport equations for k and ε are solved. With these a characteristic velocity scale and a length scale can be identified resulting in the following definition for eddy-viscosity:

$$\mu_t = C_\mu(\varrho k^2/\varepsilon) \tag{14}$$

where $C_\mu = 0.09$.

The modeled forms of the equations for k and ε, in their standard or unmodified form, are written as

$$\frac{\partial}{\partial t}(\rho k) + \frac{\partial}{\partial x_j}(\rho U_j k) = -\overline{\rho u_i'' u_j''}\frac{\partial U_i}{\partial x_j} - \rho\epsilon + \frac{\partial}{\partial x_j}\left[\left(\mu + \frac{\mu_t}{\sigma_k}\right)\frac{\partial k}{\partial x_j}\right] \tag{15}$$

$$\frac{\partial}{\partial t}(\rho\epsilon) + \frac{\partial}{\partial x_j}(\rho U_j \epsilon) = C_{\epsilon 1}\frac{\epsilon}{k}\left[-\overline{\rho u_i'' u_j''}\frac{\partial U_i}{\partial x_j}\right] - C_{\epsilon 2}\rho\frac{\epsilon^2}{k} + \frac{\partial}{\partial x_j}\left[\left(\mu + \frac{\mu_t}{\sigma_\epsilon}\right)\frac{\partial \epsilon}{\partial x_j}\right] \tag{16}$$

where

$$\sigma_k = 1.0, \qquad \sigma_\epsilon = 1.3, \qquad C_{\epsilon 1} = 1.43, \qquad \text{and} \qquad C_{\epsilon 2} = 1.92 \tag{17}$$

A. Modeling of Compressibility Effects

In the equations governing the compressible turbulent flowfield, terms can be identified that are of relevance and different from those of incompressible flows.[1] From the governing equations given earlier, the terms that are unique to compressible turbulent flows (and not accounted for in incompressible models) are $\overline{\sigma_{ij}''}$, $\overline{p'(\partial u_i''/\partial x_i)}$, and $\overline{u_i''(\partial P/\partial x_i)}$, in addition to the dilatational effects on the rate of dissipation of TKE. Here $\overline{\sigma_{ij}''}$ is purely a result of Favre averaging, and at low Mach numbers it does not represent compressibility effects. Therefore, to close the system of equations, we need to suitably account for $\overline{p'(\partial u_i''/\partial x_i)}$ and $\overline{u_i''(\partial P/\partial x_i)}$. We will refer, henceforth, to the first term as the pressure dilatation term and the second term as the enthalpic production term. A detailed description of the modifications that have been proposed to model the extra dissipation due to dilatational effects is presented in Ref. 1. Here we will briefly present the form of the modifications that have been used in the comparative study presented in this paper.

From a DNS analysis of compressible flows, Zeman[2] and Sarkar et al.[3] concluded that the effect of compressibility on the turbulence structure was a dissipative one. Compressibility introduces an extra amount of dissipation (of the turbulent fluctuations) due to the nondivergent nature of the velocity fluctuations, as can be seen by examining the definition of the rate of dissipation of TKE. Following the definition of ε given in Eq. (13), we get[2,3]

$$\varrho\varepsilon = \overline{\frac{\partial u_i''}{\partial x_j}\sigma_{ij}''} \tag{18}$$

Through some mathematical manipulations the dissipation rate (of TKE) in compressible turbulent flows can be written as a sum of a solenoidal dissipation rate [the first term on the right-hand side of Eq. (19)] and a dilatational dissipation rate. Thus,

$$\varrho\varepsilon = \varrho(\varepsilon_s + \varepsilon_d) \tag{19}$$

where

$$\varrho\varepsilon_s = \mu\overline{(\omega_p''\omega_p'')}, \qquad \varrho\varepsilon_d = \tfrac{4}{3}\mu\overline{d''^2} \tag{20}$$

where ω_p'' is the fluctuation in vorticity and $d'' = \partial u_k''/\partial x_k$ is the divergence of the fluctuating velocity field.

The solenoidal dissipation rate can be thought of as the dissipation due to the regular process of cascading of energy to the smaller scales, and in the absence of dilatational effects it can be considered to be equivalent to the incompressible dissipation rate. The dilatational dissipation (also referred to as compressible dissipation) is due to the nondivergent nature of the velocity fluctuations.

The pressure dilatation $\overline{p'd''}$, where $d'' = \partial u_k''/\partial x_k$, is one of the terms that appears explicitly in the governing equations [see Eq. (5)] in the case of compressible turbulent flows due to the nondivergent fluctuating velocity field. The pressure dilatation refers to the work done due to simultaneous fluctuations in the volume of the fluid cell corresponding to the fluctuations in pressure. It can be either positive or negative and when negative represents an extra dissipation.

1. *Sarkar et al.[3] and Sarkar[10] Modifications*

Based on an analysis of the evolution of the fluctuations on an acoustic timescale Sarkar et al.[3] proposed a model for the dilatational dissipation rate, which is given as

$$\varepsilon_d = \alpha_1 \varepsilon_s M_t^2 \tag{21}$$

where α_1 is an arbitrary constant of $\mathcal{O}(1)$. The constant α_1 is determined from an analysis of the predictions made of decaying compressible turbulence.

Borrowing ideas from the modeling of the pressure–strain correlations in incompressible turbulent flows Sarkar[10] modeled the pressure dilatation term as

$$\overline{p'd''} = -\alpha_3 P_k M_t^2 + \alpha_4 \varrho\varepsilon_s M_t^2 \tag{22}$$

where $\alpha_3 = 0.4$, $\alpha_4 = 0.2$, and $M_t = \sqrt{(2k)}/a$. In addition, α_1 in Eq. (21) is set equal to 0.5. The constants are obtained from a curve fit of the model with DNS simulations.

2. *El Baz and Launder[11] Modification*

We refer to the modifications proposed by El Baz and Launder[11] as the E–L modification. The E–L modification was proposed to account for the extra rate of dissipation due to compressibility effects and one of the constants was chosen in the modeled form of the transport equation for ε_s. The transport equation in its modeled form is given by Eq. (16). El Baz and Launder[11] chose to modify

the constant $C_{\varepsilon 2}$ to match the observed decay rate of compressible isotropic turbulence. Based on this observation, they modified this constant as

$$C'_{\varepsilon 2} = \frac{C_{\varepsilon 2}}{1 + 3.2M_t^2} \tag{23}$$

where $M_t = \sqrt{k/a}$, and used $C'_{\varepsilon 2}$ instead of $C_{\varepsilon 2}$ in the modeled form of the transport equation for ε, given in Eq. (16).

The E–L modification (for the pressure dilatation term) is obtained from a contraction of the model for the rapid part of the pressure–strain correlation as

$$\overline{p' \frac{\partial u_i''}{\partial x_i}} = F\left[\frac{8}{3}\varrho k \frac{\partial U_k}{\partial x_k} - P_k\right] \tag{24}$$

where F is the constant, which is considered to be an intrinsic function of compressibility. The function F is assumed to be a function of the turbulent Mach number; that is,

$$F = \beta M_t^2 \tag{25}$$

where $M_t = \sqrt{k/a}$ and β is an arbitrary constant whose value is prescribed to be 1.5.

3. Krishnamurty and Shyy[7] Modifications

The modifications proposed by Krishnamurty and Shyy[7] are referred to as the K–S modification. The methodology predominantly used in computing compressible flowfields is to use Favre averages for velocity components and temperature and Reynolds average for pressure and density. The stress tensor and the heat flux vector are computed using Reynolds averages. The implicit assumption here is that the turbulence is homogeneous and, therefore, the turbulent mass flux and the fluctuating stress tensor are negligible, which could be erroneous in the case of high-supersonic and hypersonic flowfields.[18] To accurately model the exact form of the governing equations (except for the dissipation rate transport equation) account must be made of the turbulent mass flux term. Krishnamurty and Shyy[7] set up a functional relationship expressing the dependence of the turbulent mass flux on the gradients in temperature and the Reynolds stresses. The functional relationship is expressed in the form

$$\overline{u_j''} = C_1\left\{\left(\frac{\mu_t C_p}{Pr_t}\right)\left(\frac{\gamma - 1}{\bar{\varrho} a^2}\right)\frac{\partial \tilde{T}}{\partial x_j} + \left[\frac{(\gamma - 1)}{\bar{\varrho} a^2}\tilde{U}_i \overline{\varrho u_i'' u_j''}\right]\right\} \tag{26}$$

where C_1 is an arbitrary constant, C_p is the specific heat at constant pressure, and

$$C_1 = 2M_t/(1 - M_t) \tag{27}$$

where $M_t = \sqrt{(2k)}/a$.

Note that the modification has been derived based on a constant enthalpy assumption (as a starting point). The mean velocity is defined with respect to a reference solid body, which in this case is the projectile.

The modeling of the transport equation for ε_s usually follows the incompressible form and ignores the effect of the baroclinic torque. Note that ε_s is usually defined as the correlation between the velocity fluctuations; that is, $\varepsilon_s = \nu \overline{\omega_i'' \omega_i''}$, where ν is the kinematic viscosity. The assumption made in the proposal for the algebraic modification for the dilatational dissipation is that the solenoidal dissipation rate is relatively unaffected in the case of compressible flows.

The exact form of the governing equation for the solenoidal dissipation rate ε_s is written as (ε in the equations that follow is used to denote the solenoidal dissipation rate ε_s)

$$\frac{\partial}{\partial t}(\varrho \varepsilon) + \frac{\partial}{\partial x_k}(\varrho U_k \varepsilon) = P_\varepsilon + D_\varepsilon + \Phi_\varepsilon - \nu \nabla^2 \varepsilon + B_\varepsilon \tag{28}$$

where

$$B_\varepsilon = 2\nu \frac{\varepsilon_{pqi}}{\varrho^2}\left\{\underbrace{\frac{\partial \varrho}{\partial x_q}\overline{\omega_p'' \frac{\partial p'}{\partial x_i}}}_{\text{term 1}} + \underbrace{\frac{\partial P}{\partial x_i}\overline{\omega_p'' \frac{\partial \varrho'}{\partial x_q}}}_{\text{term 2}} + \underbrace{\overline{\omega_p'' \frac{\partial \varrho'}{\partial x_q}\frac{\partial p'}{\partial x_i}}}_{\text{term 3}}\right\} \tag{29}$$

In the preceding equations, P_ε is the production of dissipation, D_ε the turbulent diffusion of dissipation, Φ_ε the destruction of dissipation, and ε_{pqi} the alternating tensor. The fourth term in Eq. (28) represents the viscous dissipation of ε.

B_ε [Eq. (29)] represents the baroclinic term and arises due to differences in direction between the gradients of pressure and density, i.e., the term arising due to $[\nabla(1/\varrho) \times (\nabla p)]$. In the case of the mean flow, the baroclinic term represents a production of vorticity due to the interaction of the pressure and density gradients. Based on an order of magnitude analysis,[7] the effect of the baroclinic torque is modeled as $-C_{\varepsilon 1}(\varepsilon/k)\overline{u_i''}(\partial P/\partial x_i)$. The turbulent mass flux terms appear in the transport equations for both k and ε and can be thought of as an account for both the mean and fluctuating components of the baroclinic effect.

Therefore, the modeled forms of the transport equations representing the evolution of k and ε are given as

$$\frac{\partial}{\partial t}(\varrho k) + \frac{\partial}{\partial x_j}(\varrho U_j k) = P_k - \varrho \varepsilon + \frac{\partial}{\partial x_j}\left[\left(\mu + \frac{\mu_t}{\sigma_k}\right)\frac{\partial k}{\partial x_j}\right] - \overline{u_i''}\frac{\partial P}{\partial x_i} + \overline{p' \frac{\partial u_i''}{\partial x_i}} \tag{30}$$

and

$$\frac{\partial}{\partial t}(\varrho \varepsilon) + \frac{\partial}{\partial x_j}(\varrho U_j \varepsilon) = C_{\varepsilon 1}\frac{\varepsilon}{k}\left(P_k - \overline{u_i''}\frac{\partial P}{\partial x_i}\right) - C_{\varepsilon 2}\varrho \frac{\varepsilon^2}{k} + \frac{\partial}{\partial x_j}\left[\left(\mu + \frac{\mu_t}{\sigma_\varepsilon}\right)\frac{\partial \varepsilon}{\partial x_j}\right] \tag{31}$$

where the constants are given as in Eq. (17).

B. Modeling of Nonequilibrium Effects

One of the issues of concern (even for incompressible flows) in using this form of the k–ε model is that the rate of production of TKE tends to be overpredicted and there is a lag in the response of the dissipation rate to variations in the mean strain rate. Chen and Kim[8] proposed an algebraic modification to modify the constant $C_{\varepsilon 1}$ in Eq. (16), which is given as $[1.15 + 0.25(P_k/\varepsilon)]$. Chen and Kim[8] observe that this alteration of the coefficient allows ε to respond faster to the variations in the mean strain rate. It works to enhance the development of ε when the mean strain is strong (or large production rate) and to reduce it when the mean strain is weak (or small production rate). The nonequilibrium modification due to Shyy et al.[12] and Thakur et al.[9] alters the constant $C_{\varepsilon 2}$ in the ε equation to $[1.45 + 0.45(P_k/\varepsilon)]$. This modification has been proposed[9] to be used in conjunction with $C_{\varepsilon 1}$ because of observations of the computations made of flow past a backward facing step and the hill flow inside a channel. The $C_{\varepsilon 1}$ modification reportedly overpredicts the length of the recirculating flow due to increased levels of the production of dissipation term. Further tests[19] conducted using this modification seemed to indicate an improvement in the predictions made, over the nonequilibrium modification due to Chen and Kim.[8] The standard model in its unmodified form indicates that there is an equilibrium between the production and dissipation of TKE. The $C_{\varepsilon 2}$ modification has the effect of an added timescale, which may be thought of as representing the relaxation time required for any imbalance between production and dissipation rates of TKE to return back to an equilibrium situation. Previous studies on homogeneous shear flows have shown that there is definitely a need for a relaxation timescale-based modification.[20] However, the modification in this form will tend to overpredict the rate of decay of TKE in the case of decaying isotropic turbulence. To avoid this, some form of a limiter needs to be applied to enable the modification to predict experimentally observed decay rates. One modification, as a temporary fix to the problem, could be (max{1.92, [1.45 + $0.45(P_k/\varepsilon)$]}).

IV. Projectile Flowfield Computations

Computations have been performed using a cell-centered, finite volume second-order upwind scheme with a multistage Runge–Kutta time stepping scheme.[21] Computations were performed to investigate the capabilities of the nonequilibrium modifications[8,9]

and the compressibility modifications. The compressibility modifications proposed by Sarkar et al.[3] and Sarkar[10] (for the compressible dissipation rate and the pressure dilatation correlation), the E–L modifications (for $C_{\varepsilon 2}$ and the pressure dilatation correlation), the K–S modifications for the turbulent mass flux (hence, the enthalpic production), and the baroclinic term are being investigated.

Hereafter we refer to the projectile forebody problem as the spike-off case and the problem with the spike and aerodisk assembly as the spike-on case. Unless specified otherwise, all spatial locations presented in this section are in inches. From the results of Crawford,[16] we know that the inflow conditions are such that the flowfield can be expected to be turbulent. The measurements of Huebner et al.[13] (used in comparing the current computational predictions) were not concerned with the nature of the flowfield.

A. Spike-Off Case

The computational domain (for the spike-off case) is shown in Fig. 4. The geometry of the projectile is obtained from the experimental study of Huebner et al.[13] The diameter of the hemisphere is 3.0 in., and the diameter of the cylinder is 4.0 in. The length of the cylinder is 4.0 in. The dome is offset from the cylindrical body with a 0.25-in.-long, 3.0-in.-diam cylindrical extension. The coordinate system is set up such that the dome of the hemisphere is at $x = -1.5$ in. (the radius of the hemisphere). The outer boundary of the computational domain extends to 6.0 in. from the cylinder surface.

The boundary conditions at the far field were fixed at the experimental inflow conditions. A freestream turbulence intensity of 0.3% was used to prescribe the turbulent kinetic energy and the dissipation rate ε in the freestream. This value is consistent with intensities of turbulence observed in most supersonic wind tunnels. At the outflow boundary, a simple extrapolation procedure was used because the flow is supersonic at this boundary. At the wall boundary, the compressible form of the wall function technique[21] was used.

1. *Nonequilibrium Modifications*

Computations made with the unmodified form of the k–ε model are denoted as Skε. The computations made using the nonequilibrium modification of Chen and Kim,[8] wherein the constant $C_{\varepsilon 1}$ is modified to $[1.15 + 0.25(P_k/\varepsilon)]$ in conjunction with the compressibility modification due to Sarkar et al.[3] for the extra dissipation due to compressibility [that is, $\varepsilon = \varepsilon_s + \varepsilon_d = \varepsilon_s(1 + M_t^2)$], are referred to as Ek$\varepsilon$1. The computations made using the $C_{\varepsilon 1}$ modification of Chen and Kim[8] and the $C_{\varepsilon 2}$ modification of Shyy et al.[12] and Thakur et al.,[9] where the constant $C_{\varepsilon 2}$ is modified to $[1.45 + 0.45(P_k/\varepsilon)]$, and the compressibility modification due to Sarkar et al.[3] are referred to as Ekε2.

Though not shown here, the variation of pressure along the stagnation line indicated a pressure jump (across the shock) comparable to that predicted by one-dimensional gas dynamics. No differences between the various modifications were observed in the predictions made of the pressure variation. Figure 5 shows a comparison between the computed values of TKE along the stagnation line. The unmodified model predicts a much higher value of TKE compared to the modified models Ekε1 and Ekε2. The effect of the nonequilibrium modifications are seen to be rather large, and experimental confirmation is needed to ascertain the effectiveness of these modifications. In the case of the axisymmetric afterbody flowfield, however, the nonequilibrium modification (Ekε2) did improve the model performance.[21] Also, the modification has been observed to substantially improve the predictions made of low-speed, recirculating flows.[19] Figure 6 shows a comparison between the predictions made by the unmodified model and the models modified to take into account the nonequilibrium effects. The rates of production and dissipation show a similar trend as far as the peak levels in P_k and ε are concerned. However, the level of production and dissipation predicted by the unmodified model is much larger than that predicted by the modified models, and the predictions made by the modified models (Ekε1 and Ekε2) are virtually identical. Let us consider the predictions made by the unmodified model at a given instant in time. The rate of production is about three times the rate of dissipation and so results in a substantial increase in the rate of production of dissipation term in the ε equation (using the $C_{\varepsilon 1}$ modification). The result is an increase in the predicted value of dissipation rate, and when this magnitude of dissipation rate is added to the k equation, it results in a decrease in the predicted value of k and the eddy viscosity. The

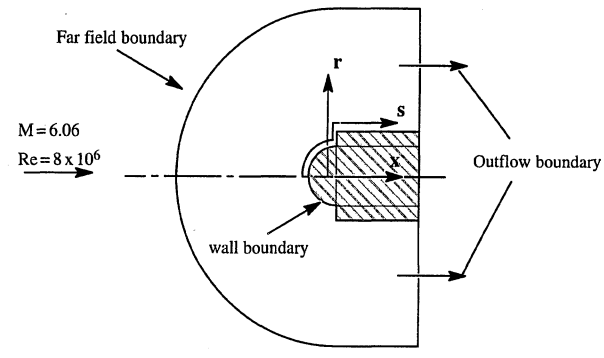

Fig. 4 Computational domain with inflow conditions.

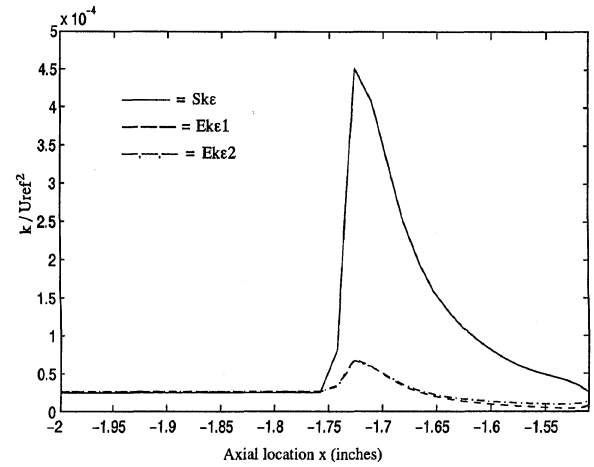

Fig. 5 Computed variation of TKE for the spike-off case.

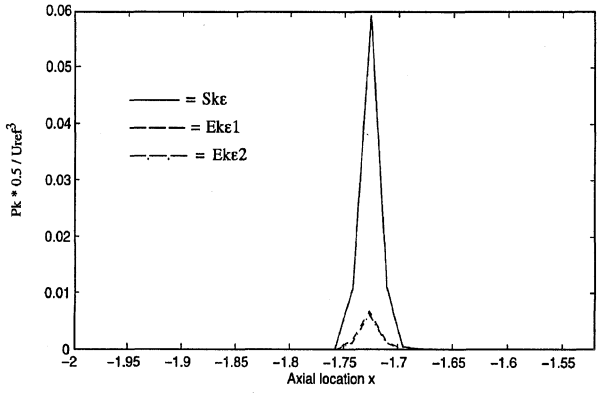

Production

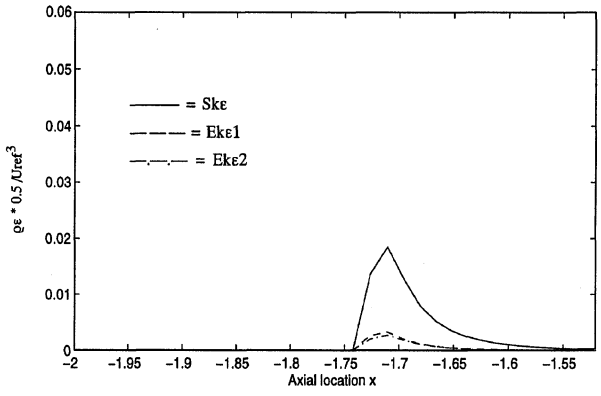

Dissipation

Fig. 6 Variation of the rates of production and dissipation of TKE along the stagnation line for the spike-off case.

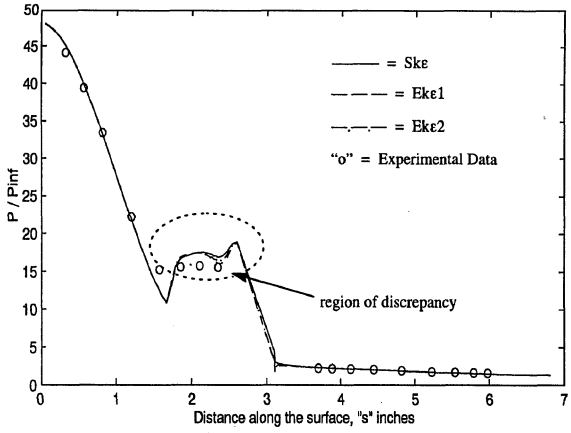

Fig. 7 Comparison of computed values of pressure with experimental data.

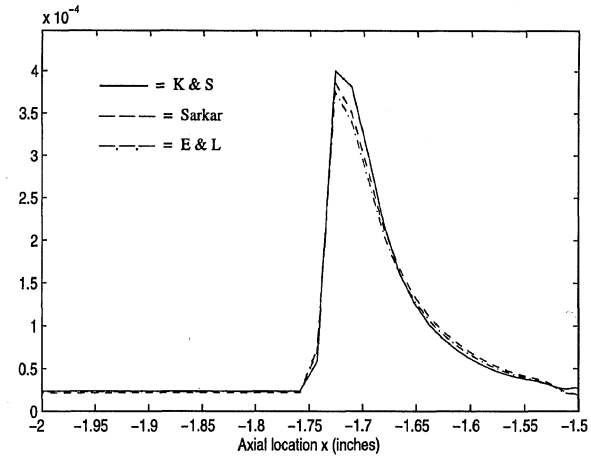

Fig. 8 Computed variation of TKE for the spike-off case.

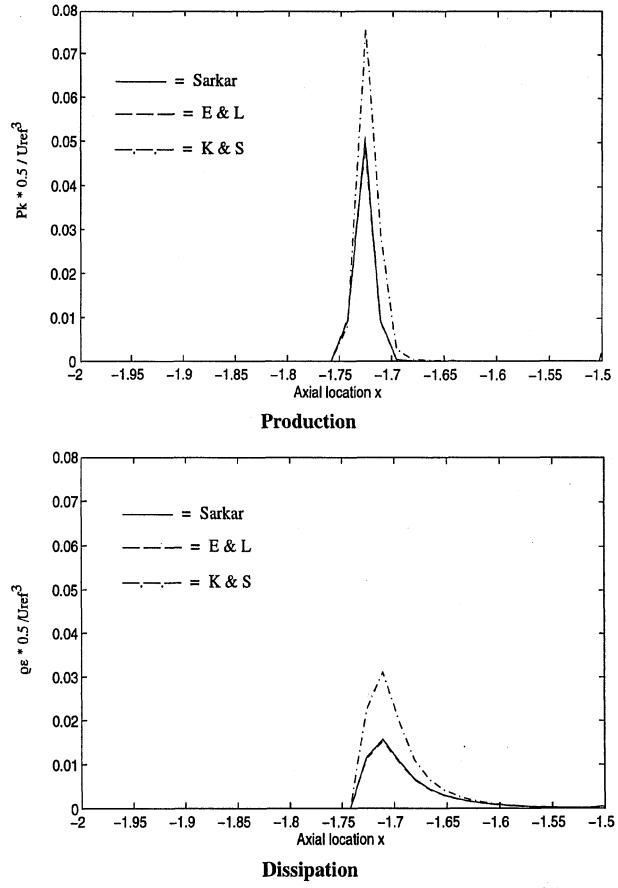

Fig. 9 Variation of rates of production and dissipation of TKE along the stagnation line for the spike-off case.

reduction in eddy viscosity leads in turn to a reduction in viscous stresses and, thereby, a reduction in the production rate. As the flow evolves, it results in substantially reduced values of TKE, ε, and P_k. In Fig. 6, the locations of the peak levels indicate that the peak in the dissipation rate is displaced one cell downstream from the peak in the production rate. It is difficult to explain this behavior.

Figure 7 shows a plot of the pressure distribution on the surface of the projectile and a comparison of the predicted values with experimental data. The predictions made by the various models are nearly identical to one another, which could be expected because there is an equilibrium between the production and dissipation in the log-layer of the boundary layer on the surface of the projectile. The compressibility modification does not play a major role because the flow is almost subsonic downstream of the shock. A possible difference between the predictions made by the models could be expected in the region where the boundary layer separates. But the differences seen in the predictions made are very minimal.

In Fig. 7, a region of discrepancy between the experimental measurements and the computational predictions has been highlighted. The jump in pressure is because of the separation of the boundary layer on the dome surface. To accommodate this separation the flow goes through a weak compression wave. The shadowgraphs and schlieren pictures of the flowfield clearly indicate this weak compression wave. But the pressure taps on the dome of the hemispherical surface fail to pick up this jump. The experimentalists Huebner et al.[13] confirmed that there is a weak compression wave but could not account for the experimentally observed pressure distribution. Other computational studies, provided by Huebner, have also confirmed the jump in pressure.

2. Compressibility Modifications

Computations using the compressibility modifications of Sarkar et al.,[3] Sarkar,[10] and El Baz and Launder[11] for the extra dissipation due to compressibility effects and the pressure dilatation correlation and the compressibility modifications for the turbulent mass flux and the baroclinic term proposed by Krishnamurty and Shyy[7] were performed to compare and contrast their effectiveness and applicability. It was observed in the computational study of the base flowfield that the E–L modifications were overly dissipative, resulting in unsatisfactory predictions of the afterbody flowfield.[7]

Figure 8 presents a plot of the predicted values of TKE along the stagnation line. The comparison between the various compressibility modifications does not show any distinct difference between the various modifications but the E–L modification does seem to predict consistently lower levels of TKE (Ref. 7).

Figure 9 presents a comparative plot of that predicted values of rate of production and dissipation of TKE along the stagnation line. The values predicted by the K–S modifications and that predicted by the Sarkar et al.,[3] Sarkar,[10] models are virtually identical. To understand the reason for this, let us consider the production of TKE:

$$\text{production of TKE} = -\overline{\varrho u_i'' u_j''}\frac{\partial U_i}{\partial x_j} - \overline{u_i''}\frac{\partial P}{\partial x_i} \tag{32}$$

where the first term on the right-hand side is termed the kinetic part and the second term the enthalpic part. The kinetic part can be further split up into a dilatational part and an isovolumetric part with the dilatational part reflecting the effect of bulk dilatation on the rate of production of TKE as follows.

Dilatational part:

$$P_{kd} = \left(\frac{1}{3}\overline{\varrho u_k'' u_k''}\right)\frac{1}{\bar{\varrho}}\frac{\mathrm{D}\varrho}{\mathrm{D}t} \tag{33}$$

Isovolumetric part:

$$P_{kiv} = \left[\left(\overline{\varrho u_i'' u_j''} - \tfrac{1}{3}\overline{\varrho u_k'' u_k''}\delta_{ij}\right)\left(S_{ij} - \tfrac{1}{3}U_{k,k}\delta_{ij}\right)\right] \tag{34}$$

Enthalpic part:

$$-\overline{u_i''}\frac{\partial P}{\partial x_i} \tag{35}$$

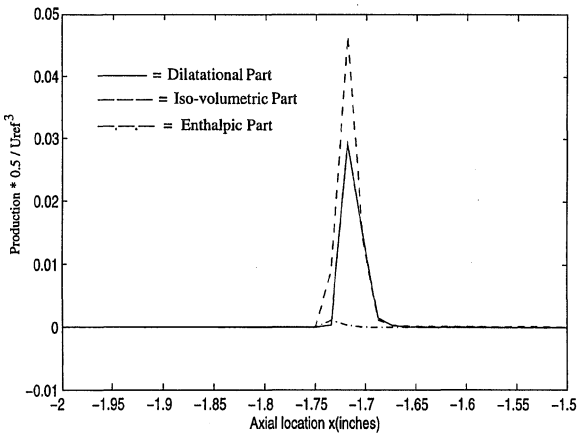

Fig. 10 Variation of the three parts of production of TKE along the stagnation line.

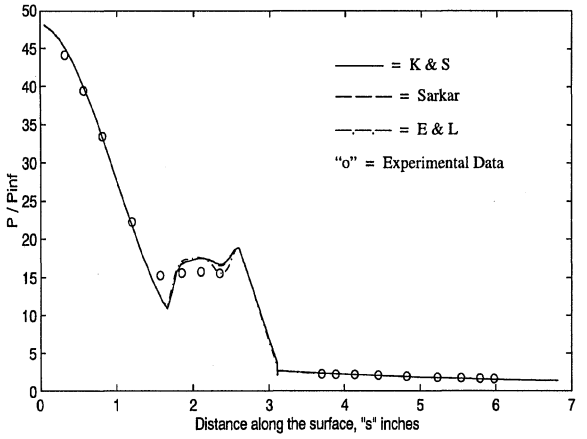

Fig. 11 Comparison of computed values of pressure with experimental data.

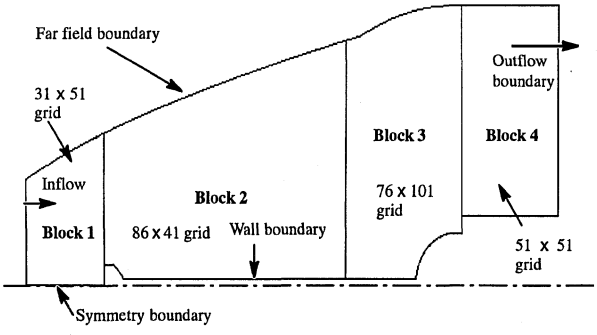

Fig. 12 Computational domain for the spike-on case with the grid system employed.

A plot of the enthalpic production rate compared with the dilatational component of the production rate and the isovolumetric part of the production rate (Fig. 10) shows that the enthalpic production rate as predicted by the current modification is not the same order of magnitude as the other two parts of the production, which explains the minor impact of the current modifications on the mean flow solution.

There is no appreciable difference seen in the predictions, made of the surface pressure distribution, by the various models that address the effect of compressibility on the turbulent flowfield, as can be seen from Fig. 11.

B. Spike-On Case

Figure 12 shows the computational domain used in the calculations. The geometry of the spike and the projectile are obtained from the experimental study of Huebner et al.[13] The domain extends

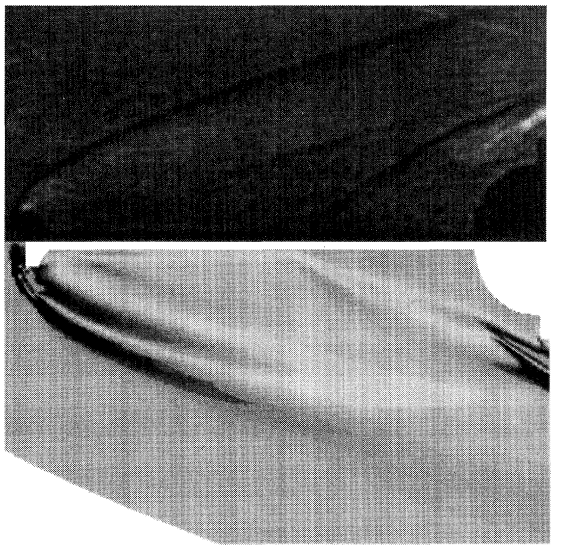

Fig. 13 Comparison of experimental schlieren with computed (K–S model) value of density gradient in the radial direction: a) experimental schlieren value and b) computed value.

about 6 in. from the top of the cylinder surface. The geometry of the projectile is the same as the one described in the preceding subsection. The length of the spike–aerodisk assembly is 12 in., and the inflow boundary is at a distance 3 in. from the aerodisk surface. The diameter of the aerodisk is 1.156 in., and the diameter of the spike is 0.375 in. The computational domain had to be split into four blocks to achieve a reasonable distribution of grid points. The blocks have continuous grid lines and so there was no need for any special interface treatment except the conservation of fluxes at interfaces. Though not presented here (for the sake of brevity) grid independence of the solution has been ascertained for the grid system shown in Fig. 12.

At the inflow boundary the inflow Mach and Reynolds numbers were specified, and the pressure and temperature were held constant. The inflow Mach and Reynolds numbers are 6.06 and 8.0×10^6, respectively. The Reynolds number is based on the projectile diameter. At the far-field boundary and at the outflow boundary a simple variable extrapolation was used. At the wall boundary the compressible form of the wall function technique has been used. At the symmetry boundary the gradients of axial component of velocity, temperature, density, TKE, and ε in the radial direction and the radial component of the velocity were set to zero.

Figure 13 shows representative contour plots of the radial gradient in density, and this is compared with the experimental schlieren photographs. The features of the flowfield are clearly seen. Figure 13a is the experimental schlieren from the measurements of Huebner et al.[13] Figure 13b was computed using the K–S model. As the flow behind the bow shock expands around the aerodisk, a weak compression is formed at its base. The wake flow caused by the aerodisk and the nearly stagnant flow near the dome create the conically shaped recirculation region. The region is separated from the inviscid flow by a flow separation shock. It is expected that this shock will isolate the recirculation region, thereby enabling the reduction of pressure and heating rates on the dome surface. Additional pockets of recirculation region are created at the shoulder region between the hemispherical dome and the cylindrical body of a larger diameter.

Figure 14 presents a comparison between the pressure distributions on the dome surface, with and without the spike and aerodisk combination. The results presented in Fig. 14 are those obtained with the K–S modifications. It is quite clear that the spike–disk combination certainly helps in reducing the pressure on the projectile surface. The decrease in pressure is almost 10 times the value obtained in the spike-off case. The distribution of temperature on the surface of the projectile, with and without the spike, is shown in Fig. 15. Even though there is substantial reduction in pressure, the use of the aerospike does not change the temperature level in the

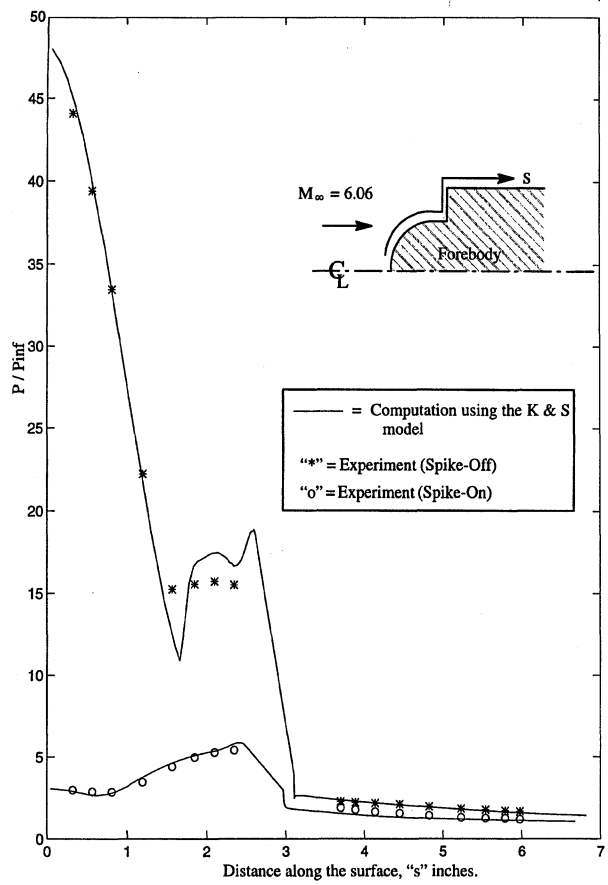

Fig. 14 Comparison of the pressure distributions on the projectile surface, with and without the spike, computed with the K–S model.

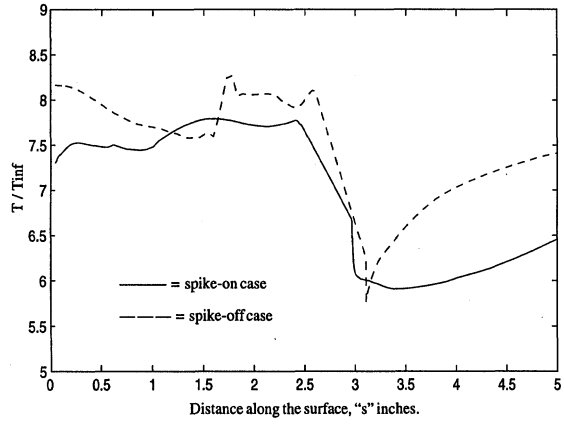

Fig. 15 Comparison of the temperature distributions on the projectile surface, with and without the spike, computed with the K–S model.

dome region substantially. Relative to the bow shock of the spike-off case, the oblique shocks of the spike-on case do not affect the thermal profile as much. However, the temperature on the dome of the projectile remains fairly constant in the spike-on case, which is desirable. Note that the current computations were restricted to an angle of attack of 0 deg. Huebner et al.[13] have reported that there is a limited range (in terms of angle of attack) of application of the spike–aerodisk combination.

1. Nonequilibrium Modifications

Computational studies of the afterbody flowfield indicated that the nonequilibrium modification of Shyy et al.[12] and Thakur et al.[9] when used in conjunction with the nonequilibrium modification of Chen and Kim[8] and the compressibility modification of Sarkar et al.[3] resulted in an optimum prediction. The predictions in the afterbody case gave reasonable predictions of both the mean flow quantities

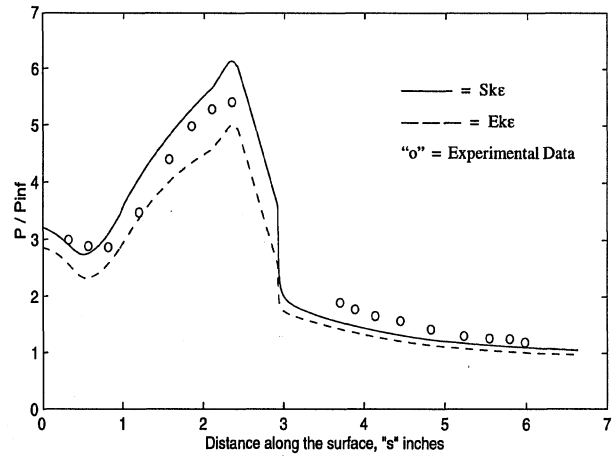

Fig. 16 Pressure distribution along the surface of the projectile, comparing nonequilibrium modification with unmodified model.

and the turbulence quantities, such as the TKE and the Reynolds shear stress. With this in mind, we decided to compare only this combination of nonequilibrium modifications (with the compressibility modification of Sarkar et al.[3]) against the predictions made by the unmodified model. The combination of nonequilibrium modifications with the compressibility modification of Sarkar et al.[3] is referred to as Ekε2.

Figure 16 presents a comparison between the predictions made of the pressure distribution on the surface of the projectile. There is a distinct difference between the predictions made by the eddy-viscosity models and the experimental data, which could be expected because the variations in pressure on the surface are dictated largely by the mechanism at play in the recirculating region. The pressure distributions on the dome surface show distinct differences between the two models, with the unmodified model predicting a much higher value of pressure on the surface of the projectile and the extended model predicting a lower value of pressure.

To compare the effectiveness of the modifications in predicting the mean flowfield, comparisons were made at three select locations along the spike. These locations are at an $x/D = -2.25$, -1.50, and -0.90. The $x/D = -2.25$ location corresponds to a location just outside the conical recirculation region. The $x/D = -0.90$ location corresponds to about the midway point of the recirculation region. Profile plots of the components of velocity and the TKE are presented in Fig. 17, which shows a lateral shift in the peak locations very similar to the shift seen in the predictions made of the afterbody flowfield.[7] However, in the afterbody flowfield case, the combination of nonequilibrium modifications yielded a prediction comparable to the prediction made using the unmodified model. The nonequilibrium-based modification of Chen and Kim[8] revealed marked shifts in the location peak values (in comparison with the unmodified model). The lateral shift seen in these computations is presumably due to the dominating influence of the $C_{\varepsilon 1}$ modification.

Figure 17 shows profile plots of the axial and radial velocity components and the level of TKE, at the three locations mentioned. There is no difference in the predictions made using the two models at the $x/D = -2.25$ location. There are substantial differences seen at the other two locations, with the standard model predicting a much higher level of TKE due to the larger rate of production of TKE predicted by the standard model. Again, due to the lack of experimental information, these comparisons are purely qualitative.

2. Compressibility Modifications

The modifications of Sarkar et al.,[3] the modifications of Sarkar,[10] those due to El Baz and Launder,[11] and the modifications proposed by Krishnamurty and Shyy[7] (that is, the modifications for the enthalpic production term and the baroclinic term) are compared. In Figs. 18 and 19, the modifications due to Sarkar et al.[3] and Sarkar[10] are denoted as Sarkar. The K–S modifications are used in conjunction with the modification for compressible dissipation rate proposed by Sarkar et al.[3]

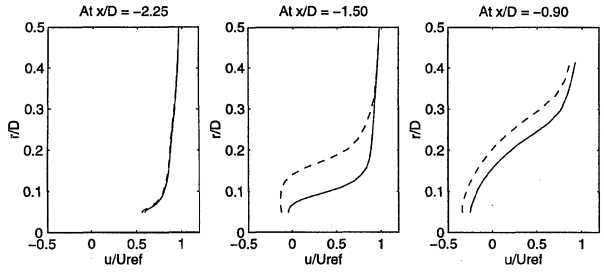

a) Computed values of axial velocity component

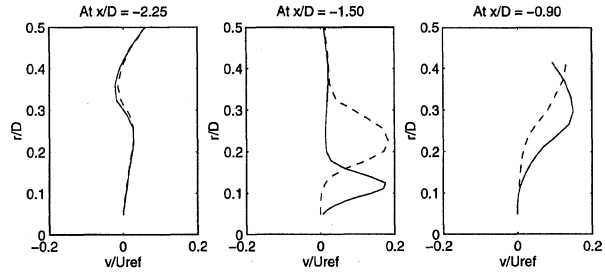

b) Computed values of radial velocity component

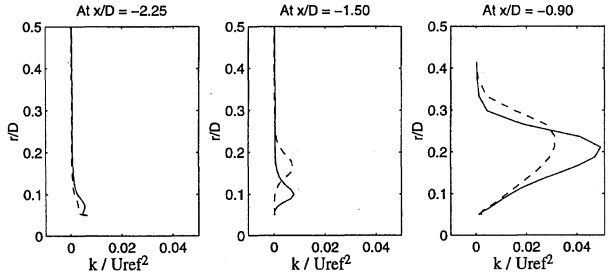

c) Computed levels of TKE

Fig. 17 Comparison of predictions made by the unmodified model and the extended model: ——, Skε and – – –, Ekε.

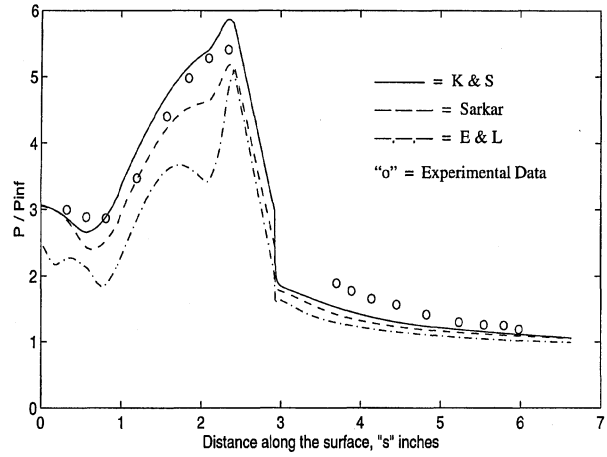

Fig. 18 Comparison of the compressibility modifications: pressure distribution along the projectile surface.

Figure 18 shows a comparison between the predictions made, using the compressibility modifications, of the pressure distribution along the surface of the projectile. The K–S modifications offer a slight improvement over the other two modifications with the possible implication that the K–S modifications are a step in the right direction.

Figure 19 presents profile comparisons, of the compressibility modifications, at the three locations along the spike, mentioned earlier. The E–L modification predicts the lowest level of TKE in the flowfield. The K–S modifications predict an increased level of TKE, which is again very similar to our observations for the afterbody flowfield.[7] The reduced level of TKE predicted by the modifications due to E–L modifications is largely due to the increased dissipation rates predicted by that model. A lateral shift in the location

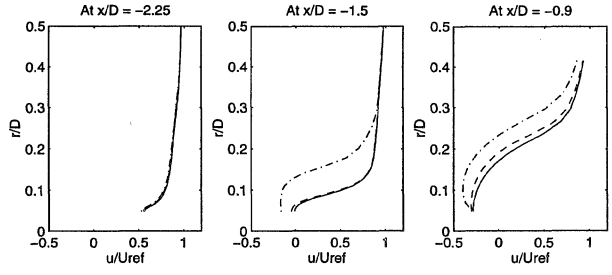

a) Computed values of axial velocity component

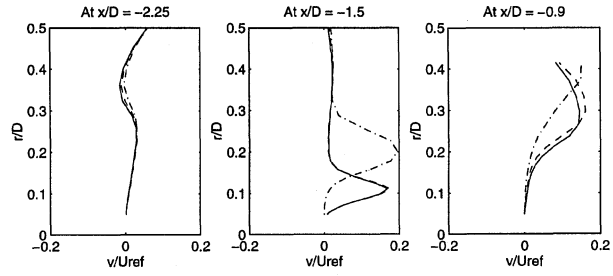

b) Computed values of radial velocity component

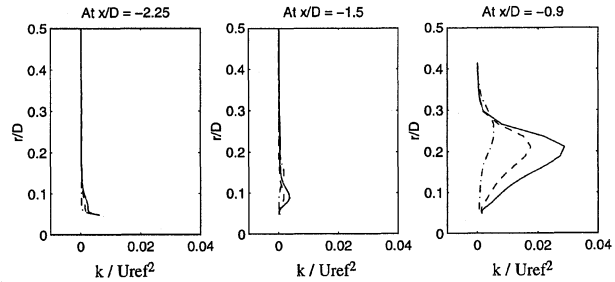

c) Computed level of TKE

Fig. 19 Comparison of predictions made using the compressibility modifications: ——, K–S; – – –, Sarkar; and –·–, E–L.

of peak values is observed in the computations made using the E–L model.

V. Summary

Modifications that have been proposed to address the issue of nonequilibrium between the rate of production and dissipation have been tested for the projectile forebody flowfield. Because of the lack of sufficient experimental measurements of this flowfield, the comparisons had to be qualitative. The standard model predicts higher rates of production of TKE, across the shock wave, in comparison with the nonequilibrium models. There are still some unresolved issues and conflicting observations (between experiment and DNS). With more insight into the phenomenon of the shock–turbulence interaction, the validity of the predictions made by the various models can be ascertained.

The modifications that have been proposed to address the effect of compressibility on the turbulent flowfield have been tested to evaluate their effectiveness and capability. In terms of the pressure distributions, on the projectile forebody surface there are no marked differences between the various models. However, the E–L modification does consistently overpredict the rate of dissipation.[1]

The use of the spike–aerodisk assembly, in front of the projectile, does reduce the pressure at the projectile surface (by almost a factor of 10). The temperature distributions on the projectile surface do not display such a dramatic reduction. However, there is a significant rise in temperature at the separation-shock location (on the surface of the spike).

For the spike-on case, the Ekε2 model (combination of the modifications for $C_{\varepsilon 1}$, $C_{\varepsilon 2}$, and compressible dissipation ε_d) predicts a longer recirculating region. The K–S modifications predict a pressure distribution that is closer to the experimental data. The modifications also predict higher values of TKE in comparison with the modifications of Sarkar et al.[3] and Sarkar.[10] The E–L modifications

predict the lowest levels of TKE, indicative of the overly dissipative nature of these modifications.

Acknowledgments

The authors would like to thank Lawrence Huebner at NASA Langley Research Center and Ellis Boudreaux at the U.S. Air Force Wright Laboratory, Armament Directorate, Eglin Air Force Base, for their valuable comments.

References

[1]Shyy, W., and Krishnamurty, V. S., "Compressibility Effects in Modelling Complex Turbulent Flows," *Progress in Aerospace Sciences* (to be published).

[2]Zeman, O., "Dilatation Dissipation: The Concept and Application in Modelling Compressible Mixing Layers," *Physics of Fluids A*, Vol. 2, No. 2, 1990, pp. 178–188.

[3]Sarkar, S., Erlebacher, G., Hussaini, M. Y., and Kreiss, H. O., "The Analysis and Modelling of Dilatational Terms in Compressible Turbulence," *Journal of Fluid Mechanics*, Vol. 227, 1991, pp. 473–493.

[4]Sarkar, S., and Lakshmanan, B., "Application of a Reynolds-Stress Turbulence Model to the Compressible Shear Layer," *AIAA Journal*, Vol. 29, No. 5, 1991, pp. 743–749.

[5]Wilcox, D. C., *Turbulence Modelling for CFD*, DCW Industries, Inc., La Cañada, CA, 1992, pp. 183–189.

[6]Huang, P. G., Bradshaw, P., and Coakley, T. J., "Turbulence Models for Compressible Boundary Layers," *AIAA Journal*, Vol. 32, No. 4, 1994, pp. 735–740.

[7]Krishnamurty, V. S., and Shyy, W., "Study of the k–ε Based Modelling of Compressible Turbulent Flows," *Physics of Fluids*, Vol. 9, No. 9, 1997, pp. 2769–2788.

[8]Chen, Y. S., and Kim, S. W., "Computation of Turbulent Flows Using an Extended k–ε Turbulence Closure Model," NASA CR 179204, Oct. 1987.

[9]Thakur, S. S., Wright, J. F., Shyy, W., Liu, J., Ouyang, H., and Vu, T., "Development of Pressure-Based Composite Multigrid Methods for Complex Fluid Flows," *Progress in Aerospace Sciences*, Vol. 32, No. 4, 1996, pp. 313–375.

[10]Sarkar, S., "The Pressure Dilatation Correlation in Compressible Flows," *Physics of Fluids A*, Vol. 4, No. 12, 1992, pp. 2674–2682.

[11]El Baz, A. M., and Launder, B. E., "Second-Moment Modelling of Compressible Mixing Layers," *Engineering Turbulence Modelling and Experiments*, edited by W. Rodi and F. Martelli, Elsevier Science B. V., Florence, Italy, 1993, pp. 63–72.

[12]Shyy, W., Thakur, S. S., Ouyang, H., Liu, J., and Blosch, E. L., *Computational Techniques for Complex Transport Phenomena*, Cambridge Univ. Press, New York, 1997, pp. 175–187.

[13]Huebner, L. D., Mitchell, A. M., and Boudreaux, E. J., "Experimental Results on the Feasibility of an Aerospike for Hypersonic Missiles," AIAA Paper 95-0737, Jan. 1995.

[14]Stalder, J. R., and Nielsen, H. V., "Heat Transfer from a Hemisphere-Cylinder Equipped with Flow-Separation Spikes," NACA TN 3287, Sept. 1954.

[15]Bogdonoff, S. M., and Vas, I. E., "Preliminary Investigations of Spiked Bodies at Hypersonic Speeds," *Journal of the Aerospace Sciences*, Vol. 26, 1959, pp. 65–74.

[16]Crawford, D. H., "Investigation of the Flow over a Spiked-Nose Hemisphere Cylinder at a Mach Number of 6.8," NASA TN D-118, Dec. 1959.

[17]Schlichting, H., *Boundary Layer Theory*, McGraw–Hill, New York, 1968.

[18]Ristorcelli, J. R., "A Representation for the Turbulent Mass Flux Contribution to Reynolds Stress and Two-Equation Closures for Compressible Turbulence," NASA CR 191569, Nov. 1993.

[19]Vu, T. C., Boyer, B., and Shyy, W., "Draft Tube Loss Prediction by Viscous Flow Analysis—The Quest for Accuracy," Proceedings of the 1996 Hydro Power Conf., Beijing, PRC, 1996.

[20]Bernard, P. S., and Speziale, C. G., "Bounded Energy States in Homogeneous Turbulent Shear Flow—An Alternative View," *Journal of Fluids Engineering*, Vol. 114, No. 1, 1992, pp. 29–39.

[21]Krishnamurty, V. S., "Effect of Compressibility on the Turbulence Structure and Its Modelling," Ph.D. Dissertation, Dept. of Aerospace Engineering, Mechanics, and Engineering Science, Univ. of Florida, Gainesville, FL, 1996.

C. G. Speziale
Associate Editor